Distributions of C_2 and C_3 radical densities in laser-ablation carbon plumes measured by laser-induced fluorescence imaging spectroscopy

K. Sasaki,[a] T. Wakasaki, S. Matsui, and K. Kadota
Department of Electronics, Nagoya University, Nagoya 464-8603, Japan

(Received 24 September 2001; accepted for publication 3 January 2002)

We measured temporal variations of the distributions of C_2 and C_3 radical densities in carbon plumes produced by laser ablation of graphite in ambient He gas. Laser-induced fluorescence imaging spectroscopy was used for the measurement. The temporal variations of total numbers of C_2 and C_3 contained in plumes were evaluated by integrating the density distributions. The experimental observations have shown that the gas-phase production of C_2 is comparable to the direct production from the target, while C_3 is mainly produced in gas phase by three-body reactions between C and C_2. In addition, we have discussed a scenario for the temporal evolution of heavy clusters (C_n with $n \geqslant 4$). The present results are useful for understanding initial formation processes of carbon clusters in laser-ablation plumes. © *2002 American Institute of Physics.*
[DOI: 10.1063/1.1455151]

I. INTRODUCTION

Unique properties and potential applications of carbon clusters such as fullerenes[1] and nanotubes[2] has led researchers to investigate the synthesis of clusters. Nevertheless, fundamental understanding of growth processes of carbon clusters is still insufficient. In order to develop an optimized synthesis method of clusters, we should have a better understanding of the formation mechanisms. However, experimental investigation on the fundamental aspect of the cluster formation is not an easy task.

Laser ablation of a graphite target in rare gas atmosphere is a synthesis method of carbon clusters.[3–7] Although the laser ablation technique is not suitable to mass production, it is useful for investigating the growth processes of clusters.[8–10] The purpose of the present work is to understand the initial growth processes of carbon clusters in carbon plumes produced by laser ablation of graphite. In this study, a diagnostic technique plays an essential role. Since kinetics of laser ablation plumes contain dynamic phenomena with transient properties, the diagnostic technique should have high temporal and spatial resolutions.

Optical methods are suitable for the diagnostics of laser-ablation plumes because of the nonintrusive nature. However, simple optical emission spectroscopy does not provide sufficient information since optical emission from the plume is obtained for only several microseconds after the irradiation of the laser pulse for ablation. In the present work, we adopted laser-induced fluorescence (LIF) imaging spectroscopy.[11–13] Using this technique, we visualized the distributions of C_2 and C_3 radical densities in laser-ablation carbon plumes. The visualized density distributions were obtained as a function of time after the irradiation of the laser pulse for ablation. The temporal variations of the total numbers of C_2 and C_3 contained in the plume were evaluated by integrating the spatial distributions. By referring to these experimental observations, we compared the gas-phase productions of C_2 and C_3 with the direct productions from the graphite target. In addition, the growth processes of clusters were discussed by considering the temporal variations of the density distributions. The present experimental results are consistent with the result of laser photoionization[14] carried out in the same apparatus. The present LIF imaging spectroscopy and the previous laser photoionization measurement provide a scenario for the evolution of carbon clusters in the laser-ablation plume.

II. EXPERIMENT

Laser ablation of graphite was carried out in a vacuum chamber shown in Fig. 1. A graphite target was installed on a rotating target holder. The electric potential of the target holder was floating. Nd:YAG laser pulses at a wavelength of 1.06 μm irradiated the target from the normal direction to the target surface. The YAG laser beam was focused using a lens, and the laser fluence on the target surface was estimated to be 3 J/cm^2. The duration of the YAG laser pulse was 10 ns. After the vacuum chamber was evacuated below 5×10^{-7} Torr using a turbomolecular pump, He gas was injected into the chamber. The pressure of ambient He gas was below 5 Torr in the present experiment.

Tunable laser pulses yielded from an optical parametric oscillator (OPO) were launched into the plume in front of the target. The tunable laser beam was arranged to have a plane shape using two cylindrical lenses. The width and the thickness of the plane-shaped tunable laser beam were approximately 27 and 1 mm, respectively. C_2 and C_3 radicals in the plume were excited by the tunable laser. Fluorescence emissions yielded from excited C_2 and C_3 formed images on the plane-shaped tunable laser beam. The images of the fluorescence emissions were taken by a charge coupled device camera with a gated image intensifier. Interference filters with high transmissions at the fluorescence wavelengths were in-

[a]Electronic mail: sasaki@nuee.nagoya-u.ac.jp

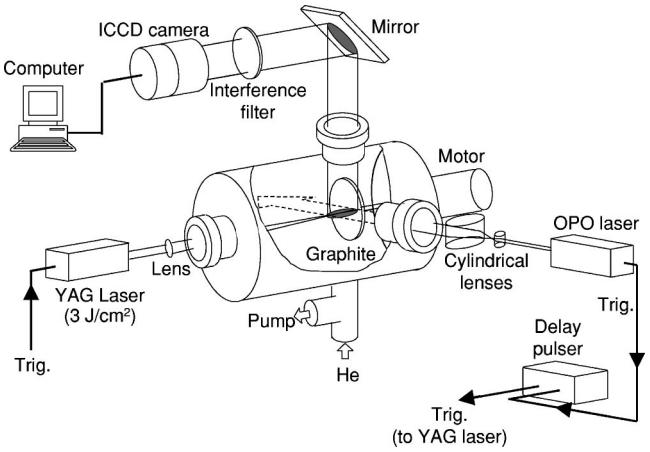

FIG. 1. Schematic of the experimental apparatus.

stalled in front of the camera to separate the fluorescence emissions from stray lights and self-emissions of the plume. In this way, we obtained the two-dimensional images of the C_2 and C_3 radical densities in the plume. The temporal variations of the density distributions were obtained by changing the delay time t_D between the oscillations of the YAG and OPO lasers. The energy levels and the wavelengths used in the present LIF imaging spectroscopy were summarized in Table I.[15–17] It is noted that C_2 radicals detected by the present LIF scheme are at a metastable ($a\ ^3\Pi_u$) state. However, since the energy separation between the $a\ ^3\Pi_u$ state and the ground ($X\ ^1\Sigma_g^+$) state is only 0.076 eV, the $a\ ^3\Pi_u$ state is expected to have a large population and to have similar characteristics to the ground state.[18] Since the wavelengths of the LIF emissions were far from the excitation wavelengths, no stray light was mixed in the images of the LIF emissions. Self-emissions of the plume at the same wavelengths as the fluorescence emissions were observed. The self-emissions were intense just after the irradiation of the YAG laser pulse. In this case, we subtracted the images of the self-emissions from those of the LIF emissions to evaluate the density distributions of C_2 and C_3 at the ground states.

III. RESULTS

A. Density distributions of C_2 and C_3 in vacuum

Figure 2 shows distributions of C_2 radical density observed at $t_D=1.5$ and 4 μs after the irradiation of the YAG laser pulse. Bird's-eye graphs are shown together with contour plots of the density distributions. The YAG laser pulse was irradiated at $r=z=0$ cm in the figure (r and z stand for the radial position and the distance from the target, respectively). Although the absolute C_2 density is unknown, the

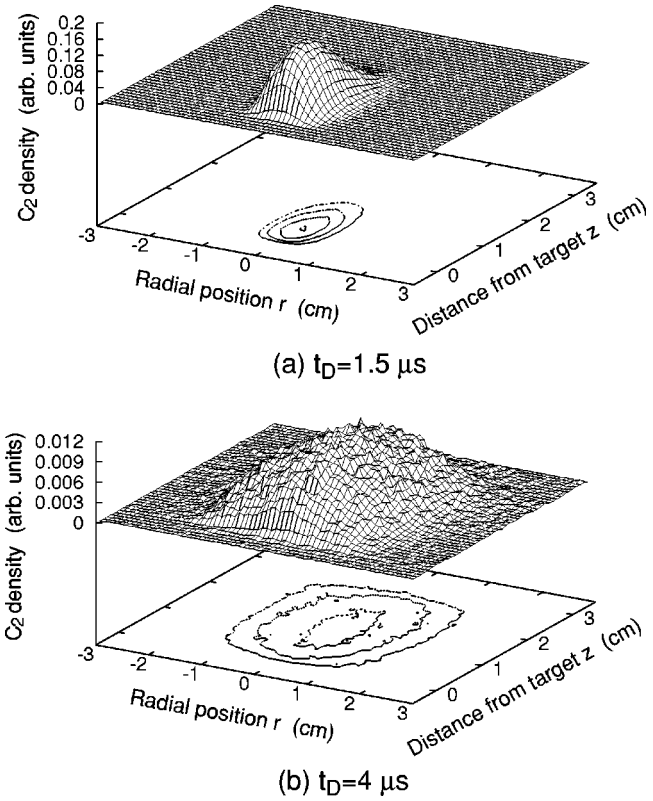

FIG. 2. Temporal variation of the density distribution of C_2 observed in vacuum.

relative change in the C_2 density can be seen from the magnitudes of the vertical axes of the figures. The magnitudes of the vertical axes of all the figures showing the distribution of C_2 density are normalized by the maximum C_2 density observed in vacuum (the maximum C_2 density in vacuum was observed at $t_D=0.6$ μs). It is seen from Fig. 2 that the density distribution of C_2 spreads rapidly after the irradiation of the YAG laser pulse. The flight speed of the peak position of the density distribution was approximately 1.5×10^5 cm/s. Because of the rapid expansion of the plume, the C_2 density at $t_D=4$ μs was one order of magnitude lower than that at $t_D=1.5$ μs.

The distributions of C_3 radical density at $t_D=1.5$ and 4 μs are shown in Fig. 3. The maximum C_3 density in vacuum was observed at $t_D=1.5$ μs. The magnitudes of the vertical axes of all the figures showing the distribution of C_3 density are normalized by the maximum C_3 density in vacuum at $t_D=1.5$ μs. The vertical axes of Figs. 2 and 3 cannot be compared. The ratio of C_2 to C_3 densities have not been determined yet. Since the C_3 density observed in vacuum is low, Fig. 3 is poor in the signal-to-noise ratio. The rapid

TABLE I. Energy levels and wavelengths used in the LIF imaging spectroscopy.

Particle	Initial state	Excitation	Excited state	Fluorescence	Final state
C_2	$a\ ^3\Pi_u(v''=0)$	516.52 nm ⟶	$d\ ^3\Pi_g(v'=0)$	563.6 nm ⟶	$a\ ^3\Pi_u(v''=1)$
C_3	$\tilde{X}\ ^1\Sigma_g^+(000)$	405.13 nm ⟶	$\tilde{A}\ ^1\Pi_u(000)$	426.4 nm ⟶	$\tilde{X}\ ^1\Sigma_g^+(100)$

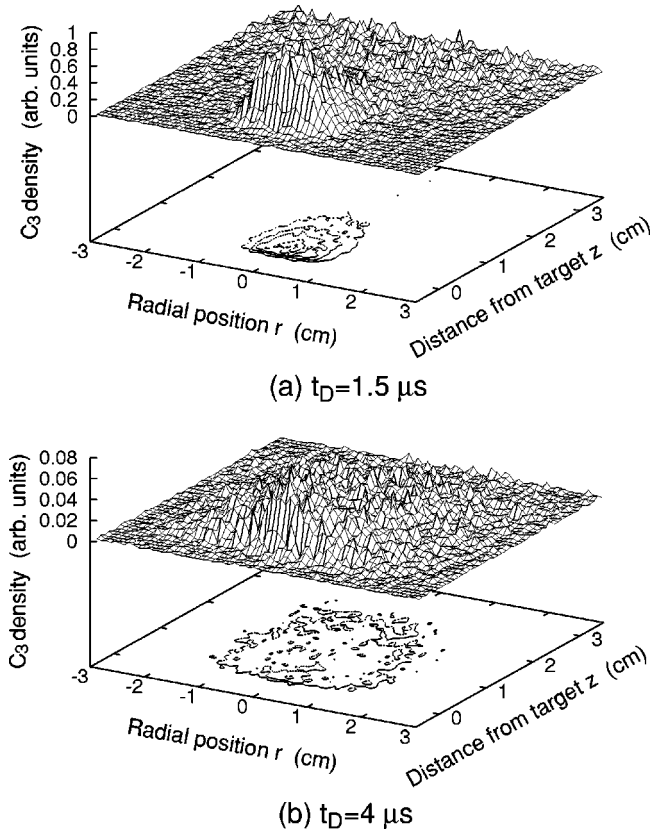

FIG. 3. Temporal variation of the density distribution of C_3 observed in vacuum.

expansion of the density distribution was also observed in C_3. At $t_D=4\ \mu$s, the C_3 radical density was close to the noise level.

B. Density distributions of C_2 and C_3 in ambient He gas at 1 Torr

The distributions of C_2 radical density at $t_D=4$, 20, and 100 μs observed in ambient He gas at 1 Torr are shown in Fig. 4. In ambient He gas at a pressure higher than 0.5 Torr, the expansion and the movement of the plume were restricted significantly, and the entire volume of the plume existed inside of the observation area for a long time. Comparing Fig. 4(a) with Fig. 2(b), it is known that the volume of the plume in ambient He gas was much smaller than that in vacuum at the same observation time. Because of the restricted expansion of the plume, the C_2 radical density observed in ambient He gas was much higher than that observed in vacuum. The density distribution of C_2 shown in Fig. 4(a) has a crescent shape with a sheer front and a gradually decreasing tail. This crescent density distribution may be owing to a shock wave (blast wave) which is excited by the supersonic expansion of the high-density plume in ambient He gas.[19] The crescent density distribution disappeared after $t_D\simeq 10\ \mu$s. The movement of the plume was very slow after the disappearance of the shock wave, and the density distribution of C_2 approached the isotropic one as shown in Figs. 4(b) and 4(c). The slow expansion of the density distribution after $t_D=10\ \mu$s may be mainly due to diffusion.

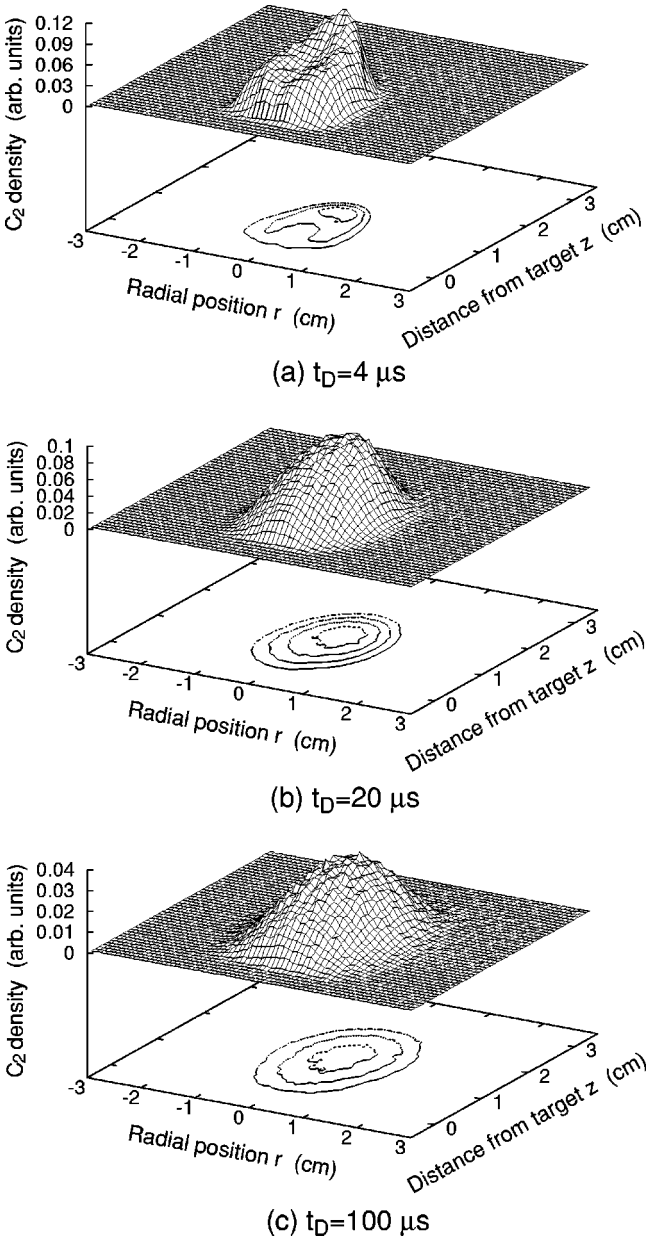

FIG. 4. Temporal variation of the density distribution of C_2 observed in ambient He gas at 1 Torr.

Figure 5 shows the distributions of C_3 radical density observed in ambient He gas at 1 Torr. The magnitudes of the vertical axes of Fig. 5 indicate that the C_3 density in ambient He gas was higher than the maximum C_3 density in vacuum. As shown in Fig. 5(a), the distribution of the C_3 density at $t_D=20\ \mu$s had two peaks. A peak was adjacent to the target surface, and the other peak was located near the leading edge of the plume. Comparing Fig. 5(a) with Fig. 4(b), it is seen that the peak near the leading edge roughly corresponds to the peak position of the C_2 density at the same observation time of $t_D=20\ \mu$s. At $t_D=100\ \mu$s, we observed the growth of the peak near the leading edge. On the other hand, the peak adjacent to the target decreased with time as shown in Figs. 5(b) and 5(c).

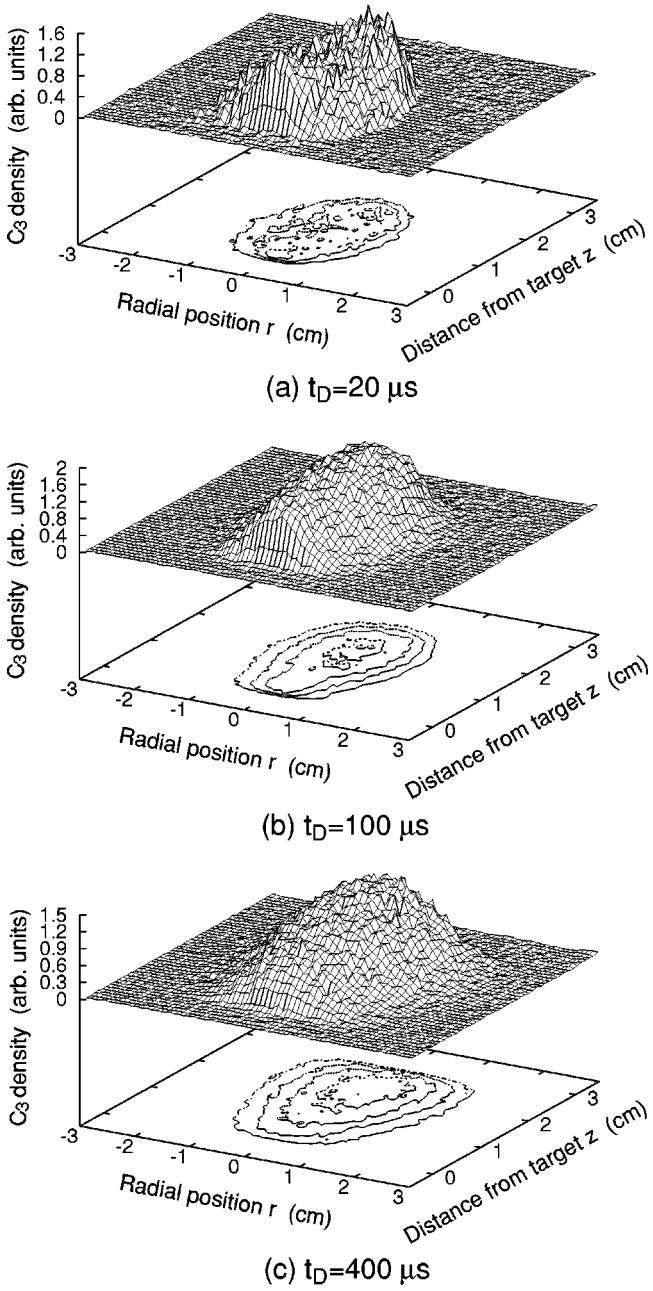

FIG. 5. Temporal variation of the density distribution of C_3 observed in ambient He gas at 1 Torr.

C. Density distributions of C_2 and C_3 in ambient He gas at 5 Torr

In ambient He gas at 5 Torr, the movement and the expansion of the plume were restricted more significantly. In comparison with Fig. 4, the size of the density distribution of the C_2 radical in 5 Torr was smaller than that in 1 Torr at the same observation time. In addition, the C_2 density in 5 Torr was higher than that in 1 Torr. The crescent density distribution due to the excitation of a shock wave was also observed in ambient He gas at 5 Torr at $t_D \leqslant 8$ μs. At $t_D \leqslant 20$ μs, the peak in the density distribution of C_2 was positioned at the front area of the plume as shown in Figs. 6(a) and 6(b). On the other hand, at $t_D = 100$ μs, the peak in the density distribution was neighboring to the target. The C_2 density decreased at $t_D \geqslant 20$ μs. The decrease in the C_2 density was significant in the front area of the plume, resulting in the particular density distribution shown in Fig. 6(d).

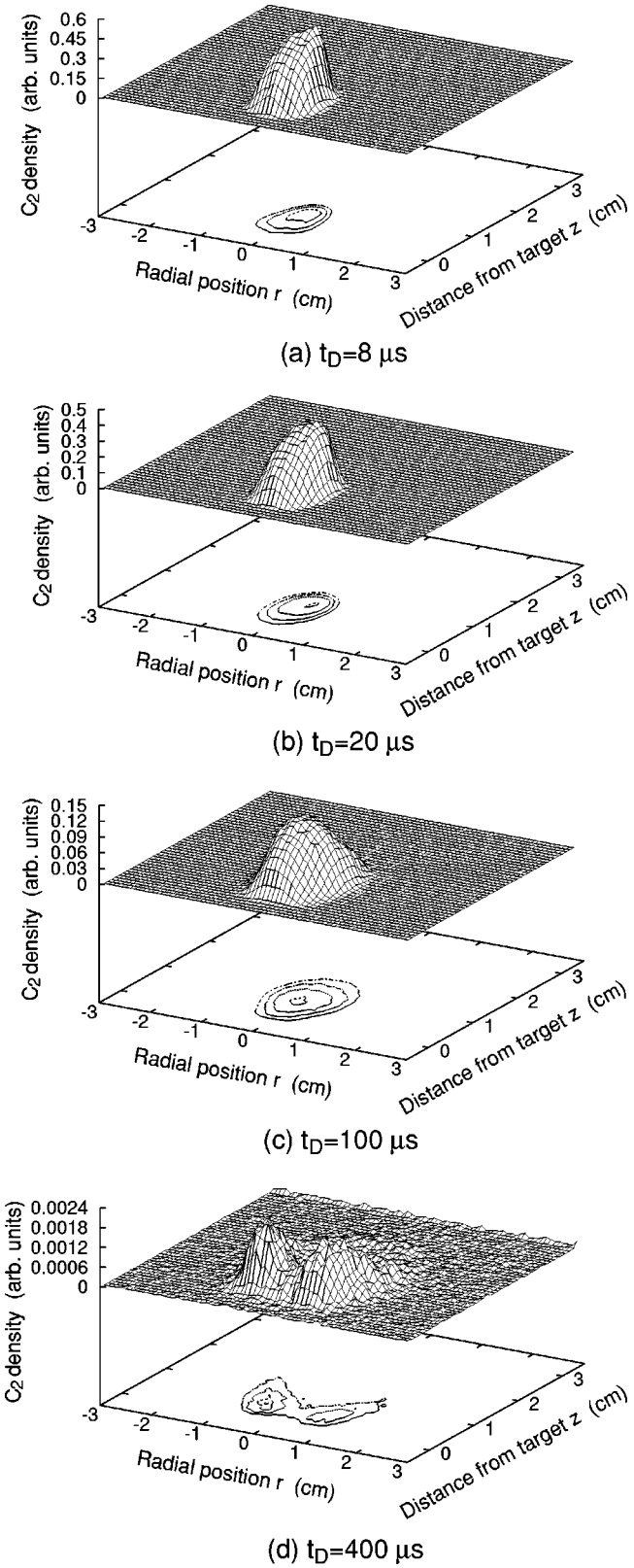

FIG. 6. Temporal variation of the density distribution of C_2 observed in ambient He gas at 5 Torr.

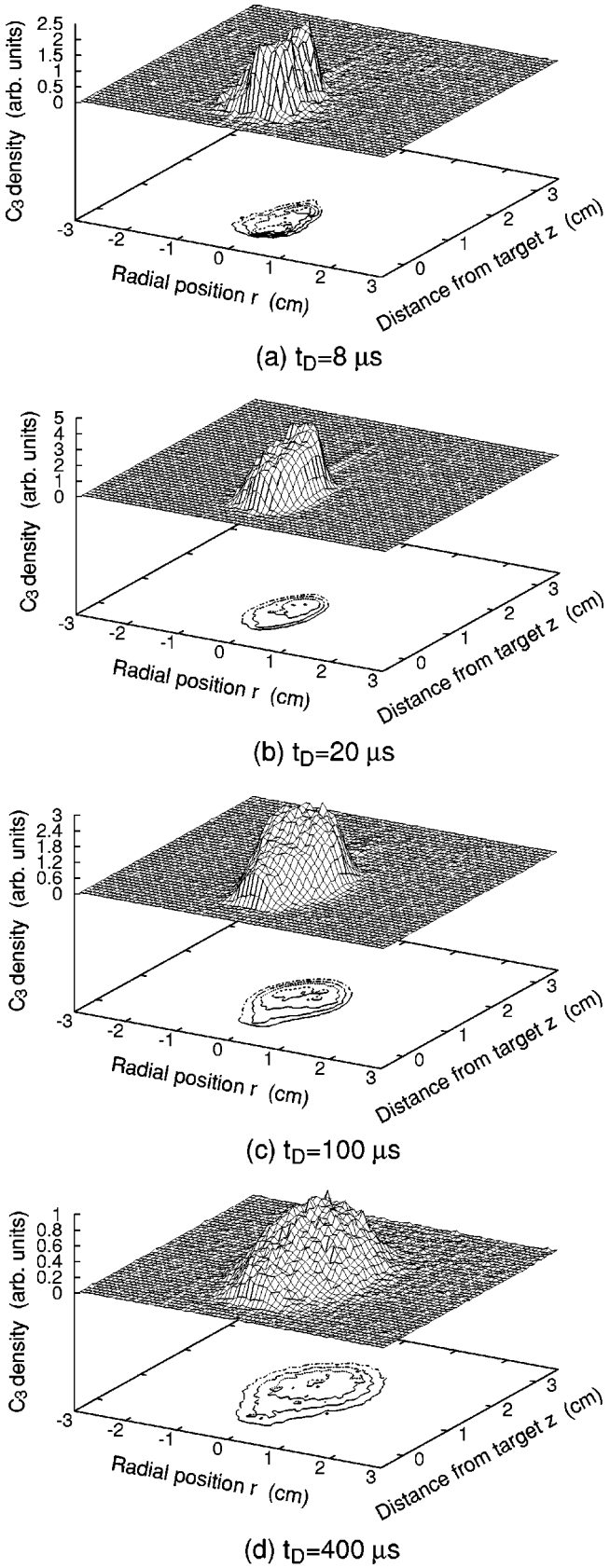

FIG. 7. Temporal variation of the density distribution of C_3 observed in ambient He gas at 5 Torr.

The size of the density distribution of C_3 in 5 Torr was also smaller than that in 1 Torr as shown in Fig. 7. The peak C_3 density in 5 Torr was higher than that in 1 Torr at $t_D \leqslant 200\ \mu$s. The double peak structure of C_3 radical density was also observed in He gas at 5 Torr as shown in Fig. 7(a). The growth of the peak in the front area of the plume was remarkable, while the peak adjacent to the target decreased monotonically. These different behaviors of the two peaks resulted in the density distribution of C_3 having the peak in the front area of the plume as shown in Figs. 7(c) and 7(d). It is noted that the growth area of the C_3 density corresponds to the decreasing area of the C_2 density. Comparing Fig. 7(d) with Fig. 6(d), it is known that the C_2 and C_3 radicals occupy different areas in the plume at $t_D = 400\ \mu$s.

IV. DISCUSSION AND CONCLUSIONS

A. Influence of collisional quenching

The intensity of LIF emission is influenced by collisional quenching under high-pressure (high-density) conditions. In the case of the present experiment, the quenching of the LIF emissions from C_2 and C_3 is caused by collisions with ambient He gas and with particles ejected from the target. The quenching due to collision with He is expected to be spatially uniform. To examine the influence of the quenching due to collision with He, we measured the lifetimes of LIF emissions from C_2 and C_3 as a function of the pressure. This measurement was carried out at a delay time of $t_D = 100\ \mu$s to avoid the quenching due to collision with ejected particles. As a result, it was confirmed that the quenching of the LIF emission from C_2 due to collision with He was negligible at pressures less than 5 Torr, while we observed the decrease in the lifetime of C_3 with the He pressure. From the pressure dependence of the lifetime, we evaluated a radiative lifetime of 210 ns and a quenching rate coefficient of 3×10^{-11} cm^3/s for the $\tilde{A}\,^1\Pi_u(000)$ state of C_3. From this experimental result, the decrease in the LIF emission intensity from C_3 is corrected by multiplying the raw LIF intensity by a factor of $(1+0.2p)$ with p being the He gas pressure in Torr. On the other hand, the correction of the quenching due to collision with ejected particles is difficult. This is because the quenching due to collision with ejected particles is dependent on the position since ejected particles have significant spatial distributions as shown in Figs. 2–7. According to the decrease in the lifetime observed at $z = 10$ mm from the target, the quenching due to collision with ejected particles decreases the LIF emission intensity at $t_D \leqslant 5\ \mu$s. The influence of the quenching is more significant in the neighboring region to the target. It is noted that the influence of collisional quenching has not been corrected in Figs. 2–7 because of the difficulty in the correction of the quenching due to collision with ejected particles. The details of the experimental results on the collisional quenching will be described in a separate paper.[20]

B. Comparison between reactions and transport

The dynamic behaviors of the density distributions of C_2 and C_3 are determined by the combined effect of transport and reactions. It is known from Figs. 2 and 3 that, in vacuum

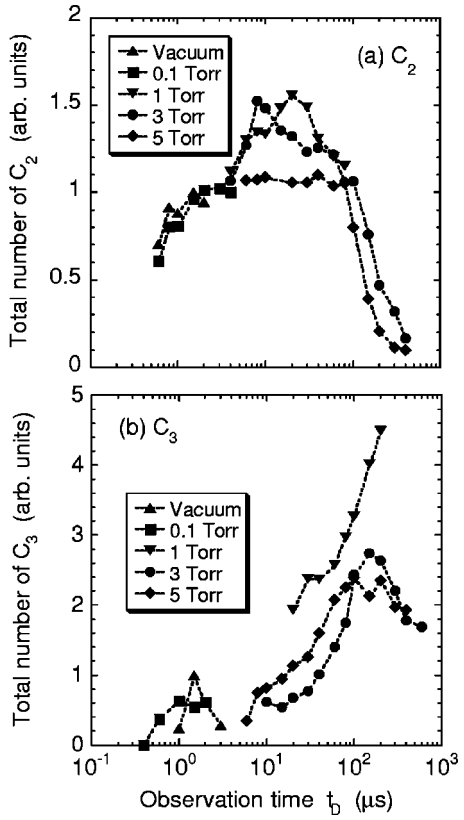

FIG. 8. Temporal variation of the total numbers of (a) C_2 and (b) C_3 contained in the plume.

and ambient He gas at low ($\leqslant$0.1 Torr) pressures, transport is principally important in the determination of the C_2 and C_3 radical densities. Because of the rapid transport, the C_2 density in vacuum decreases by a factor of 100 at 4 μs after the irradiation of the YAG laser pulse. In ambient He gas at pressures higher than 0.5 Torr, hydrodynamic effects such as the excitation of a shock wave partly influence the density distributions of C_2 and C_3. However, chemical reactions predominantly govern the behaviors of C_2 and C_3 when the chamber is filled with ambient He gas. This is because the transport of the plume is significantly restricted by collision between ablated particles and He gas. As shown in Figs. 4–7, C_2 and C_3 are lost inside of the observation area due to chemical reactions.

C. Temporal change in the total numbers of C_2 and C_3

In order to examine the effect of reactions in the plume separately, we spatially integrated the density distributions shown in Figs. 2–7 to evaluate total numbers of C_2 and C_3 contained in the plume. The integration was carried out only when the entire volume of the density distribution was located in the observation area. The density distributions measured experimentally in both sides of $r \geqslant 0$ cm and $r \leqslant 0$ cm were averaged. The distribution thus obtained in the (r,z) plane was integrated under the assumption of the cylindrical symmetry. The temporal variations of the total numbers of C_2 and C_3 radicals are shown in Fig. 8. The magnitudes of the vertical axes of Figs. 8(a) and 8(b) are normalized by the maximum numbers of C_2 and C_3, respectively, observed in vacuum. In other words, the vertical axes show the degree of the enhancement in the numbers of C_2 and C_3 in gas phase, provided that the numbers of C_2 and C_3 ejected from the target directly are independent of the pressure of ambient He gas. It is noted that the quenching of the LIF emissions due to collision with particles ejected from the target may be responsible for the small total numbers of C_2 and C_3 observed at $t_D \leqslant 5$ μs.

As shown in Fig. 8(a), the numbers of C_2 observed in ambient He gas at 1 and 3 Torr were 1.6 times bigger than that in vacuum at the maximum. The increase in the number of C_2 is probably due to a gas-phase reaction,

$$C + C + M \rightarrow C_2 + M. \quad (1)$$

The ambient He gas enhances this three-body reaction by increasing the density of M in two ways; one is the increase in the density of He and the other is the increase in the local density of carbon species. The latter effect is obtained by the fact that the expansion of the plume is restricted in ambient He gas. The peak in the total number of C_2 appeared at $t_D \simeq 8$ μs in 3 Torr, which was earlier than the peak time of $t_D \simeq 20$ μs observed in 1 Torr. This result is reasonable since reaction (1) is more efficient in ambient gas at a higher pressure. On the other hand, the total number of C_2 observed in 5 Torr was smaller than those in 1 and 3 Torr. However, the smaller number of C_2 in 5 Torr may not indicate the less efficient production of C_2. The production of C_2 is probably efficient in 5 Torr, but the loss of C_2 may also be significant. The loss of C_2 means the production of heavier carbon species C_n with $n \geqslant 3$. The constant number of C_2 observed at $t_D = 7-60$ μs in 5 Torr may be attributed to the balance between the production and the loss of C_2. In the decreasing period of the total number, C_2 is consumed by the production of heavier carbon species.

As shown in Fig. 8(b), the enhancement in the total number of C_3 in ambient He gas was more significant than that of C_2. The quenching of the LIF emission due to collision with He is corrected in Fig. 8(b). In ambient He gas at 1 Torr, the total number of C_3 was 4.5 times bigger than that in vacuum. The increasing period of the total number of C_3 corresponded to the decreasing period of the total number of C_2. These results suggest the gas-phase production of C_3 due to a reaction,

$$C_2 + C + M \rightarrow C_3 + M. \quad (2)$$

This three-body reaction becomes more efficient in ambient He gas at a higher pressure. The production of C_3 from C_2 is supported by the fact that the increasing area of C_3 corresponds to the decreasing area of C_2 as shown in Figs. 4–7. The total numbers of C_3 observed in 3 and 5 Torr were smaller than that in 1 Torr, which may be due to the significant loss of C_3 to produce heavier carbon species.

D. Main sources of C_2 and C_3

According to the discussion described above, the main sources of C_2 and C_3 are identified as follows. It is generally understood that gas-phase productions of C_2 and C_3 due to

reactions (1) and (2) are negligible in vacuum and a low gas pressure. Therefore the main sources of C_2 and C_3 in the low-pressure (<0.1 Torr) condition are the graphite target. In ambient He gas at a pressure higher than 0.5 Torr, the three-body reactions (1) and (2) become efficient. However, since the increase in the total number of C_2 is approximately 60% at the maximum as shown in Fig. 8(a), the graphite target plays the principal role as the source of C_2 even in ambient He gas at a high pressure. This means that C_2 is a major species ejected from the graphite target by laser ablation. On the other hand, since the increase in the total number of C_3 by a factor of 4.5 is observed in ambient He gas, the predominant source of C_3 is not the target but the gas phase. The gas-phase production of C_3 in ambient He gas dominates the direct ejection from the graphite target.

E. A scenario for the temporal evolution of carbon clusters

The temporal variations of the total numbers of C_2 and C_3 give us a rough scenario for the evolution of carbon clusters in a plume produced by laser ablation of a graphite target in ambient He gas. At $t_D \leqslant 5\ \mu$s, the plume moves from the irradiation point of the YAG laser pulse. The speed of the plume is decelerated by collision with ambient He gas, and the movement of the plume almost stops at $t_D \simeq 5\ \mu$s. During the movement and the expansion of the plume, a shock wave is excited. After $t_D \simeq 5\ \mu$s, the dynamics of the plume is governed by chemical reactions. At $5 \leqslant t_D \leqslant 10\ \mu$s, C_2 radicals are produced by reaction (1), which is the first step of the cluster formation. The production of C_3 radicals by reaction (2) follows the production of C_2 at $10 \leqslant t_D \leqslant 200\ \mu$s. In this period, the total number of C_2 decreases. At $t_D \geqslant 200\ \mu$s, the total numbers of C_2 and C_3 decrease, which may correspond to the formation of heavier clusters by reactions such as $C_2 + C_m + M \rightarrow C_{m+2} + M$, $C_3 + C_n + M \rightarrow C_{n+3} + M$, and $C_m + C_n + M \rightarrow C_{m+n} + M$. As described in a previous paper,[14] we have carried out the detection of heavy carbon clusters in the plume using a laser photoionization technique. As a result, we have observed the increase in the cluster signal at $0.1 \leqslant t_D \leqslant 4$ ms. Therefore the speculation from the present experimental results that heavy clusters are mainly formed at $t_D \geqslant 200\ \mu$s is consistent with the previous photoionization diagnostics of the plume. It is noted that the time scale described here is probably dependent on experimental conditions. For example, if the pressure of ambient gas is higher, the size of the plume may be smaller due to the confinement effect of the ambient gas, which may result in the faster growth of clusters. An important point shown by the present work is the sequential growth of clusters.

[1] H. W. Kroto, J. R. Heath, S. C. O'Brien, R. F. Curl, and R. E. Smalley, Nature (London) **318**, 162 (1985).
[2] S. Iijima, Nature (London) **358**, 220 (1992).
[3] T. Guo, P. Nikolaev, A. Thess, D. T. Colbert, and R. E. Smalley, Chem. Phys. Lett. **236**, 419 (1995).
[4] M. Yudasaka, T. Komatsu, I. Ichihashi, Y. Achiba, and S. Iijima, J. Phys. Chem. B **102**, 4892 (1998).
[5] H. Kataura, A. Kimura, Y. Ohtuka, S. Suzuki, Y. Maniwa, T. Hanyu, and Y. Achiba, Jpn. J. Appl. Phys., Part 2 **37**, L616 (1998).
[6] F. Kokai, K. Takahashi, M. Yudasaka, R. Yamada, T. Ichihashi, and S. Iijima, J. Phys. Chem. **103**, 4346 (1999).
[7] D. B. Geohegan, H. Scittenhelm, X. Fan, S. J. Pennycook, A. A. Puretzki, M. A. Guillorn, D. A. Blom, and D. C. Joy, Appl. Phys. Lett. **78**, 3307 (2001).
[8] K. Kaizu, M. Kohno, S. Suzuki, H. Shiromaru, T. Moriwaki, and Y. Achiba, J. Chem. Phys. **106**, 9954 (1997).
[9] K. Shibagaki, T. Kawashima, K. Sasaki, and K. Kadota, Jpn. J. Appl. Phys., Part 1 **39**, 4959 (2000).
[10] K. Shibagaki, K. Sasaki, N. Takada, and K. Kadota, Jpn. J. Appl. Phys., Part 2 **40**, L851 (2001).
[11] T. Okada, Mater. Sci. Forum **301**, 95 (1999).
[12] A. A. Puretzki, D. B. Geohegan, X. Fan, and S. J. Pennycook, Appl. Phys. Lett. **76**, 182 (2000).
[13] T. Ikegami, S. Ishibashi, Y. Yamagata, K. Ebihara, R. K. Thareja, and J. Narayan, J. Vac. Sci. Technol. A **19**, 1304 (2001).
[14] T. Kawashima, K. Sasaki, T. Wakasaki, and K. Kadota, Appl. Phys. A: Mater. Sci. Process. **69**, S767 (1999).
[15] R. W. B. Pearse and A. G. Gaydon, *The Identification of Molecular Spectra* (Wiley, New York, 1976), p. 82.
[16] L. Gausset, G. Herzberg, A. Lagerqvist, and B. Rosen, Astrophys. J. **142**, 45 (1965).
[17] K. Takizawa, K. Sasaki, and K. Kadota, J. Appl. Phys. **88**, 6201 (2000).
[18] C. Suzuki, K. Sasaki, and K. Kadota, Jpn. J. Appl. Phys., Part 1 **38**, 6896 (1999).
[19] Ya. B. Zel'dovich and Yu. P. Raizer, *Physics of Shock Waves and High Temperature Hydrodynamic Phenomena* (Academic, New York, 1966).
[20] T. Wakasaki, K. Sasaki, and K. Kadota, Jpn. J. Appl. Phys. (submitted).